New mutation in the *myocilin* gene segregates with juvenile-onset open-angle glaucoma in a Brazilian family ☆

Carolina Ayumi Braghini [a,*], Izabella Agostinho Pena Neshich [a], Goran Neshich [b], Fernanda Caroline Soardi [a], Maricilda Palandi de Mello [a], Vital Paulino Costa [c], José Paulo Cabral de Vasconcellos [c], Mônica Barbosa de Melo [a]

[a] *Centro de Biologia Molecular e Engenharia Genética (CBMEG), Universidade Estadual de Campinas, Avenida Cândido Rondon 400, Cidade Universitária "Zeferino Vaz", Distrito de Barão Geraldo, P.O. Box 6010, 13083-875, Campinas, SP, Brazil*
[b] *Empresa Brasileira de Pesquisa Agropecuária, Informática Agropecuária (Embapra-CNPTIA), Avenida André Tosello 209, Cidade Universitária "Zeferino Vaz", Distrito de Barão Geraldo, P.O. Box 6041 13083-886 Campinas, SP, Brazil*
[c] *Departamento de Oftalmologia e Otorrinolaringologia, Faculdade de Ciências Médicas, Universidade Estadual de Campinas, Rua Tessália Vieira de Camargo 126, Cidade Universitária "Zeferino Vaz", Distrito de Barão Geraldo, P.O. Box 6111 13083-970, Campinas, SP, Brazil*

ARTICLE INFO

ABSTRACT

Mutations in the *myocilin* gene (*MYOC*) account for most cases of autosomal dominant juvenile-onset open-angle glaucoma (JOAG), an earlier and more severe form of POAG. We accessed seven members of a Brazilian JOAG family by clinical and molecular investigation. Four out of seven family members were diagnosed with JOAG. All of these patients presented high intraocular pressure and two of them were bilaterally blind. The disease onset varied from 20 to 30 years old. There was a nine-year-old family member who had not yet manifested the disease, although he was also a carrier of the mutation. Ophthalmologic examination included: evaluation of the visual field and optic disc, intraocular pressure measurement, and gonioscopy. The three exons and intron/exon junctions of the *MYOC* gene were screened for mutations through direct sequencing of PCR-amplified DNA fragments. Mutation screening revealed an in-frame mutation in the third exon of the *MYOC* gene: an insertion of six nucleotides between the cDNA positions 1187 and 1188 (c.1187_1188*ins*CCCAGA, p.D395_E396*ins*DP). This mutation presented an autosomal dominant pattern of inheritance, segregating with the disease in four family members for three generations, and it was absent in 60 normal controls. We also performed a computational structure modeling of olfactomedin-like domain of myocilin protein and conducted in silico analysis to predict the structural changes in the myocilin protein due to the presence of the mutation. These findings may be important for future diagnosis of other presymptomatic family members, as well as for the increase of the panel of *MYOC* mutations and their effects on phenotype.

© 2013 Elsevier B.V. All rights reserved.

1. Introduction

Glaucoma is a heterogeneous group of optic neuropathies and is the leading cause of irreversible blindness worldwide (Fan et al., 2006; Ray et al., 2003; Shields et al., 1996). Primary open-angle glaucoma (POAG) is the most common form of glaucoma, and is characterized by slow progression of optic disc atrophy, with corresponding loss of peripheral visual field and characteristic excavated appearance of the optic disc (Quigley and Vitale, 1997). It has been estimated that approximately 58.6 million people worldwide will be affected by the disease by the year 2020 (5.9 million will be affected bilaterally) (Quigley and Broman, 2006). The increase of intraocular pressure (IOP) is often associated with POAG; therefore, it is considered a major risk factor (Quigley and Vitale, 1997; Wiggs et al., 1996).

Although the prevalence of POAG increases with age, a subgroup of patients is diagnosed with a relatively rare form of the disease, juvenile-onset open-angle glaucoma (JOAG). JOAG has an early onset, but the age limitation between the adult and juvenile onset is controversial. Nowadays, it is commonly considered that JOAG manifests between 3 and 35 years old and the initiation of the disease after this age is categorized as POAG (adult onset). In many cases, JOAG

presents a pattern of autosomal dominant inheritance, while POAG is mostly considered a complex genetic disease (Wiggs et al., 1996). JOAG patients typically have high IOP, as well as a frequent need for surgical treatment (Johnson et al., 1993; Wiggs et al., 1995).

Until now, 17 chromosomal loci have been linked to POAG and/or JOAG by linkage analysis (GLC1A to GLC1Q) (Allingham et al., 2005; Baird et al., 2005; Fingert et al., 2011; Lin et al., 2008; Monemi et al., 2005; Pang et al., 2006; Pasutto et al., 2009; Porter et al., 2011; Sarfarazi et al., 1998; Sheffield et al., 1993; Stoilova, 1996; Suriyapperuma et al., 2007; Trifan et al., 1998; Wang et al., 2006; Wiggs et al., 2004; Wirtz et al., 1997, 1999). The myocilin gene (MYOC) (region 1q23–q24, GLC1A locus), described in 1997 by Stone et al. (1997), was the first gene linked with JOAG. The myocilin protein, encoded by the MYOC gene, is a glycoprotein with 504 amino acids and a signal peptide for secretion, a leucine zipper within an N-terminal myosin-like domain, and a C-terminal olfactomedin-like domain (Ortego et al., 1997). The majority (about 85%) of more than 80 missense or nonsense mutations already found in the MYOC gene was described in the olfactomedin-like domain, the most conserved protein domain (www.myocilin.com; Hewitt et al., 2008). Myocilin can form dimers and multimers, and it is believed that this protein participates in the formation of the extracellular matrix, although its function has not yet been elucidated (Fautsch and Johnson, 2001; Jacobson et al., 2001).

Data from in vitro and in vivo studies have indicated that some mutant myocilin isoforms are not secreted, but are rather retained in the endoplasmic reticulum (ER) of the trabecular meshwork cells, causing reticulum stress and apoptosis of these cells (Jacobson et al., 2001; Joe et al., 2003; Liu and Vollrath, 2004). Different sensitivities to oxidative stress may be dependent of the type of MYOC mutation. Cells in culture expressing the p.Y437H mutant were more sensitive to apoptosis secondary to induction of oxidative stress than the p.I477N mutant (Joe and Tomarev, 2010). The increased level of oxidative stress-protective proteins as well as the increased level of pro-apoptotic protein, CHOP, were observed in transgenic mice expressing p.Y437H MYOC mutation and glaucomatous phenotype (Joe and Tomarev, 2010; Zhou et al., 2008). Also, apoptosis can be caused by aggregation of myocilin in the ER that activates unfolded protein response, an evolutionarily conserved stress pathway (Carbone et al., 2009). Myocilin is also capable of interacting with various other proteins such as Optimedin (Torrado et al., 2002), Fibronectin (Ueda et al., 2002), α1-Syntrophin (Joe et al., 2012), and some similarities between mechanisms of action of Wnt proteins and myocilin have been demonstrated (catenin-independent mechanism) (Kwon and Tomarev, 2011). Besides, myocilin may act as non-canonical Wnt signaling agent, inducing the formation of stress fibers (Kwon et al., 2009).

MYOC gene mutations are present in 8% to 36% of JOAG cases and 3% to 4% of POAG cases (Fingert, 2011). Although there is a relatively low contribution of MYOC gene mutations to the etiology of POAG, the high prevalence of this disease makes them the most important cause of blindness with a molecular basis (Stone et al., 1997). The importance of recognizing individuals with POAG carrying MYOC mutations has been transformed into the proposal for new therapeutic approaches, including the use of chemical chaperones such as Sodium 4-phenylbutarate (PBA) and the regulation of chaperones with selective inhibition of Glucose-regulated protein 94 (Grp94) (Suntharalingam et al., 2012; Zode et al., 2012). Besides, as the gain of function, rather than haploinsufficiency, is the mechanism suggested for the development of glaucoma associated with MYOC mutations, the evaluation of new disease-causing variants is important in helping to clarify their pathophysiology.

In this paper, we describe a novel in-frame mutation in the MYOC gene segregating with JOAG in three generations of a Brazilian family. In addition, we conducted in silico analyses to better understand the effects of the mutation in the protein.

2. Material and methods

2.1. Patient selection

Seven members belonging to a Brazilian family with European ancestry from Paraná, a state in the south region of Brazil, were recruited in the Glaucoma Service at the Clinical Hospital, University of Campinas, where the clinical analysis was carried out. Ophthalmic examination included IOP measurement by means of applanation tonometry; slit-lamp biomicroscopy and gonioscopy; evaluation of the optic disc with a 78-diopter lens; and automated perimetry (Humphrey System 24.2; Zeiss-Humphrey-Zeiss Systems, Dublin, CA, USA). Ocular history was obtained by interview, including the age at diagnosis of glaucoma, and clinical and surgical treatment. Diagnosis of JOAG was based on the presence of at least two of the following characteristics: (1) IOP above 21 mmHg; (2) optic disc changes, including thinning of the neuroretinal rim, hemorrhage, notch, cup-to-disc ratio greater than 0.7, or asymmetry of the cup-to-disc ratio greater than 0.2; and (3) glaucomatous visual field defect, defined as a corrected pattern standard deviation outside the 95% normal limits or a glaucoma hemifield test result outside the 99% limits. The control group consisted of 60 individuals of varying ethnicities, mostly white, from different regions of the country, also recruited in the Glaucoma Service at the Clinical Hospital, University of Campinas, according to the following criteria: absence of any form of glaucoma; absence of family history of glaucoma or blindness of unknown cause; IOPs lower than 15 mmHg; cup-to-disc ratio lower than 0.4; and older than 50 years of age. This study was approved by the research ethics committee of the Faculty of Medical Sciences, University of Campinas. The participating subjects gave informed consent, in agreement with the principles enunciated in the Declaration of Helsinki.

2.2. Mutation screening

Whole blood was collected from affected and unaffected family members and normal controls. Genomic DNA was extracted using the phenol/chloroform method (Sambrook et al., 1989) and the DNAs were precipitated with absolute ethanol. The three coding regions and intron/exon junctions of the MYOC gene were amplified by PCR, prepared with 40 to 100 ng of DNA template, 20 pmol of each forward and reverse primer (Table 1), 200 pmol of each dideoxynucleotide, 1× enzyme buffer (10× buffer: 200 mM Tris–HCl pH 8.4, 500 mM KCl), 0.5 U of Taq DNA polymerase (Invitrogen™ Life Technologies, Carlsbad, CA, USA), and ultrapure water to complete the final volume of 25 μL. The conditions of amplification were the same for all three exons of the MYOC gene, except for the annealing temperature, as specified in Table 1: initial denaturation at 95 °C for 5 min, followed by 35 cycles at 95 °C for 1 min, annealing of primers in specific temperature for each region for 45 s, and extension at 72 °C for 90 s, ending with additional extension at 72 °C for 7 min. Both strands of the MYOC gene were screened for sequence alterations by direct sequencing, with BigDye Terminator Cycle Sequencing Kit v3.1® (Applied Biosystems Inc., Foster City, CA, USA) and submitted to electrophoresis

Table 1
Forward (F) and reverse (R) primers used in the polymerase chain reaction and direct sequencing of the MYOC gene, their annealing temperature and product size.

Exon	Primer sequence (5′–3′)	Annealing temperature (°C)	Product size (bp)
1 (F)	GGTGCATAAATTGGGATGTTC	62.0	999
1 (R)	TTGTGCTAGCTGTGCAGTCTC	62.0	999
2 (F)	AACATAGTCAATCCTTGGGCC	61.0	346
2 (R)	GAGAGTTCTGTTCCTCTTCCTC	61.0	346
3a (F)	GATTTGTCTCCAGGGCTGTC	65.0	916
3a (R)	GCTTGGAGGCTTTTCACATC	65.0	916
3b (F)	TCTGTGGCACCTTGTACACC	62.0	841
3b (R)	CCACCTTTAACATCCTGCAATC	62.0	841

in the ABI Prism 3700 DNA Analyzer automated sequencer (Applied Biosystems Inc., Foster City, CA, USA). The primers used for PCR and direct sequencing were chosen based on the gene sequence deposited in GenBank (OMIM *601652) and are depicted in Table 1. Sequencing data were analyzed through the FinchTV program (Geospiza, Seattle, WA, USA) and BLAST at the NCBI server.

2.3. In silico analyses

To verify the level of conservation of the region where the mutation was detected among the species, the sequence of normal human myocilin was compared with myocilin of other species, using the program ClustalW for multiple sequence alignment (free access) (Thompson et al., 1994). Structural analysis was performed by first verifying the existence of solved structures with homologous sequences to myocilin olfactomedin-like domain (residues 235 to 504) with BLASTp searches against PDB database. As there were no significant hits, an alternative modeling procedure was employed by using the threading software I-TASSER (Zhang, 2007). The best ranked model according to I-TASSER Z-score resembled the folding of a protein whose structure is described in the PDB file 2zw9.pdb and was selected for further optimization. Jpred (Cuff et al., 1998) and PSIPRED (Buchan et al., 2010) were used to predict the type, extension and localization of secondary structure elements of olfactomedin domain because initial quality assessment of I-TASSER model indicated residues located in prohibited Ramachandran plot areas. This indication of secondary structure elements was then used as a set of restraints to a new modeling procedure performed by MODELLER 9v11 software (Sali and Blundell, 1993) which used the I-TASSER output as a template to generate improved models. As another restraint, a disulfite bridge between Cys245 and Cys433 was introduced (in accordance with experimental evidences (Nagy et al., 2003)). Obtained models were ranked by Modeller DOPE score and Ramachandran plot analysis. The best ranked model was initially refined using YASARA: the system containing the protein structure immersed in a box with water molecules (solvent) was optimized via energy minimization and molecular dynamics for 500 ps (using the macro md_refine). By this procedure any remaining steric clashes were eliminated. Molecular dynamics simulation used the AMBER03 force field and all other parameter values were set to the same values as in the original macro. The resulting structure selected as the one with the minimal energy in the molecular dynamics trajectory was then subjected to additional quality assessment using Prosa-Web (Wiederstein and Sippl, 2007), space-clash analysis and Ramachandran plot from STING platform and its Java Protein Dossier (Neshich et al., 2004, 2006). The p.D395_E396insDP and P370L mutations were introduced in the previously obtained model for wild type structure by homology modeling followed by molecular dynamics refinement via YASARA. The wild type and mutant structures were analyzed using STING Millennium (BlueStar STING) (Neshich et al., 2003) and electrostatic surface maps were created employing PyMOL (DeLano, 2002). Accessible surface areas were calculated using the software SurfV (Sridharan et al., 1992). The structures were analyzed for hydrophobicity at exposed surface through SHI algorithm (Surface Hydrophobicity Index) (Neshich et al., unpublished results).

3. Results

3.1. Phenotypic studies

A Brazilian family harboring JOAG in three generations with an autosomal dominant inheritance pattern was identified (Fig. 1). Individual II-3 was subjected to two trabeculectomies, but was bilaterally blind at age 67. The proband, his son (III-1), also lost the vision in both eyes at age 40, presenting visual acuity of 20/25 and 20/60 with tubular visual field (less than 10°). He underwent three trabeculectomies in both eyes for IOP control, but still needs to use prostaglandin analogs

to maintain IOP close to 10 mmHg. One of the proband's daughters, member IV-1, was diagnosed with JOAG at the age of 20. Since then, she has been using three medications for IOP control. However, due to two pregnancies, the clinical treatment was interrupted and her IOP rose to 30 and 28 mmHg in the right eye (RE) and left eye (LE), respectively. Her visual acuity is 20/20 in both eyes and the visual field presents with superior arcuate scotoma in RE and incomplete superior arcuate scotoma in the LE with vertical cup-to-disc ratios of 0.9 and 0.7 in the RE and LE, respectively. At this moment, IOP is under control (12 mmHg) with maximum topical medication. The other two daughters, individuals IV-2 and IV-3, have no symptom of glaucoma (Table 2), but individual IV-4 was diagnosed as ocular hypertensive at 22 years of age, with IOPs of 22 and 23 mmHg in the RE and LE, respectively. Due to his low age and the presence of risk factors for glaucoma, including the rise in IOP and family history of glaucoma, clinical treatment was initiated. Nowadays, his IOP is between 15 and 18 mmHg in both eyes, controlled with prostaglandin analogs and beta-blocker. The visual field remains unaltered and the vertical cup-to-disc ratio is 0.2 and 0.3. All members of this family presented with wide-open angle at gonioscopy, allowing visualization of ciliary band. All affected members presented with high IOP and severe disease (except individual IV-4, who is clinically controlled) that required intensive clinical treatment; in the older members of the family, more than one surgical intervention was necessary for IOP control. Mean age at diagnosis of glaucoma was 25.25, ranging from 20 to 30, characterizing the disease as JOAG. The clinical data on the family members are depicted in Table 2.

3.2. Genotypic studies

By direct sequencing, a new in-frame mutation, an insertion of six nucleotides between the cDNA positions 1187 and 1188 (c.1187_1188insCCCAGA) in the MYOC gene was identified, segregating in four individuals with the disease (II-3, III-1, IV-1, IV-4) from three generations of that particular Brazilian family (Fig. 2). This insertion
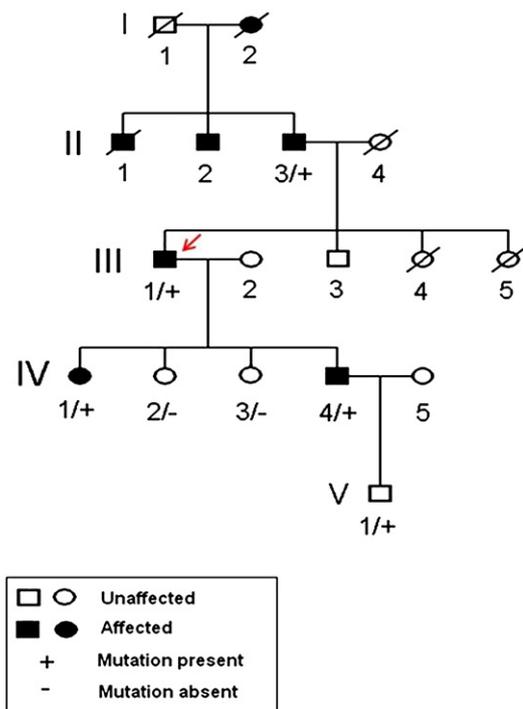

Fig. 1. Pedigree of the studied Brazilian family. The c.1187_1188insCCCAGA mutation in the myocilin gene segregates with the disease in three generations (individuals II-3, III-1, IV-1, and IV-4). The red arrow indicates the proband.

Table 2
Clinical features of the Brazilian family members according to the presence/absence of the mutation.

ID	Family member	Diagnosis	Mutation	Age/age diag. (years)	Highest IOP RE (mmHg)	Highest IOP LE (mmHg)	CD ratio RE	CD ratio LE	Surgeries/medication
II-3	Father	JOAG	Yes	77/30	34.00	34.00	1.00	1.00	2/1
III-1	Proband	JOAG	Yes	48/29	42.00	47.00	1.00	1.00	3/2
IV-1	Daughter	JOAG	Yes	23/20	30.00	28.00	0.90	0.70	–/3
IV-2	Daughter	Normal	No	12/–	16.00	16.00	0.20	0.20	–/–
IV-3	Daughter	Normal	No	21/–	14.00	14.00	0.20	0.20	–/–
IV-4	Son	JOAG	Yes	27/22	22.00	23.00	0.20	0.30	–/2
V-1	Grandson	Normal	Yes	9/–	No data	No data	0.30	0.30	–/–

Abbreviations: ID = identity, Age Diag. = age at diagnosis, Highest IOP: highest intraocular pressure; CD ratio: cup-to-disc ratio; RE = right eye, LE = left eye.

was absent in 120 chromosomes from normal controls. The insertion of six base pairs (CCCAGA) led to the putative inclusion of two amino acids, aspartic acid and proline, in the olfactomedin-like domain between the second and third bases of residue 396 (p.D395_E396insDP) of myocilin. The sequence of the protein remains the same, except for these two residues, causing an increase in the total number of amino acids in the mutated myocilin from 504 to 506 residues. The mutation is also present in an unaffected member of the family (V-1), who is only nine years old. The new variation was published in the *myocilin* variation database (www.myocilin.com; Hewitt et al., 2008).

3.3. In silico analyses

From the alignment of normal human myocilin and myocilins from other organisms: common chimpanzee, crab-eating macaque, greater galago, brown rat, house mouse, domestic cat, domestic dog, cow, horse, wild boar, European rabbit, Tasmanian devil, chicken and zebrafish (protein sequences were taken from GenBank), it is clear that neither Asp395 nor Glu396 residues are highly conserved among mammal species; however, they are located within a conserved region (Fig. 3). Molecular modeling resulted in a model structure for myocilin olfactomedin-like domain which was predominantly composed by antiparallel β-sheets, turns and disordered loops (Fig. 4). Although the mutation does not truncate the protein, it might affect the pre-existing secondary structure (according to the prediction program PSIPRED v2.6). However, there was no evident perturbation of the overall structure visible in the modeled mutant since the RMSD (root–mean–square deviation) with wild type modeled structure was only 1.1 Å.

According to the modeled structure of p.D395_E396insDP, this insertion caused reduction of accessible surface area of both Asp395 and Glu396 (from 46.6 Å^2 and 65.8 Å^2 to 15.1 Å^2 and 49.3 Å^2, respectively). Locally, there was an evident reduction of solvent exposed area built by charged and polar groups (74.7 Å^2 and 47.4 Å^2 of reduced exposed area, respectively), mainly from Gln368 and Glu357 which are located
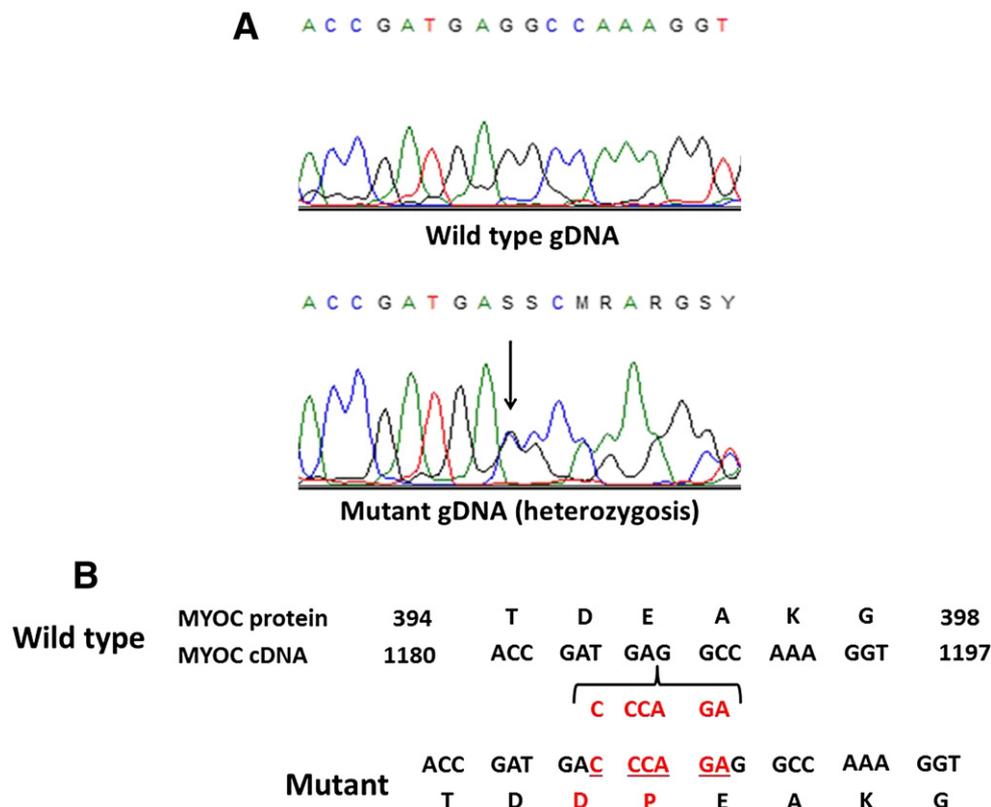

Fig. 2. Direct sequencing of the third exon of the *MYOC* gene. In A, above — an unaffected subject, with the wild type sequence of the *MYOC* gene, and below — an affected subject, showing the mutation c.1187_1188insCCCAGA in heterozygosis. The arrow indicates the location of the insertion. In B, the wild type and mutant cDNA and protein sequences, shown in red are the nucleotides and respective residues inserted.

Fig. 3. Multiple amino acid alignment of myocilin proteins, demonstrating that D395 and E396 are not highly conserved residues.

around 9 and 15 Å from the insertion site, as shown in Fig. 5A. It is possible to visualize that a neutral region emerged in the mutated structure, as indicated by a black arrow in the electrostatic surface maps of wild type and mutant olfactomedin-like domains (Fig. 5A and B). The neutral electrostatic potential may indicate that more charged groups have been buried than exposed when aspartic acid and proline were inserted. This can affect the balance of charges at the surface, and it has been suggested that reduction of the net charge is significantly associated with protein deposition diseases (Chiti et al., 2002). According to the modeled wild type structure the insertion site is located near another important residue, P370, a mutation associated with JOAG (yellow circle, Fig. 5A). The distance between P370 and the insertion site is around 8 Å. In order to check if other mutations (reported in the literature) created a similar patch of neutral electrostatic surfaces, the molecular structure of the JOAG-associated mutation P370L was modeled. The mutated residue, leucine, is a more hydrophobic residue and it assumed a position where it was exposed to a solvent at the protein surface. His366 and Tyr365 became more exposed upon mutation (with additional 11.5 Å² and 23.1 Å² surface areas, respectively). The neutral patch of the protein surface was slightly larger in the mutant than in the wild type although smaller than the observed for the mutant p.D395_E396insDP (Fig. 5C).

Since the reduced exposition to solvent of charged and polar residues at p.D395_E396insDP might indicate that neutral patches at the

Fig. 4. Overall structure of modeled olfactomedin domain of myocilin (residues 235–504) shown in sticks are the residues associated with the disease.

surface may have been formed, it is possible that these patches could be also more hydrophobic. The Surface Hydrophobicity Index (SHI) (Neshich et al., unpublished), based on Engelman scale, was calculated for the three modeled structures. The calculation of SHI is based on normalization of each amino acid residue hydropathy by their effective accessible surface area. The SHI describes the cumulative surface hydrophobicity for a selected chain. For wild type, SHI was 0.28, smaller than the values obtained for the insertion mutant and P370L mutant (0.288 and 0.283). An increased hydrophobic patch at this protein may serve as target for binding to other mutated myocilin proteins or to any other protein. It is known that low solubility and aggregation of proteins are caused by increased area of exposed hydrophobic surfaces (Horwich, 2002). Even among variants which display similar structures, the aggregation propensity can be explained by increased area of hydrophobic patches (Münch and Bertolotti, 2010).

The mutation may have also caused alterations of the internal contact networks of olfactomedin-like domain such as the overall number of charge repulsive contacts (from 13 in the wild type to 5 in the mutant model) which can also influence the protein function (Münch and Bertolotti, 2010). Several alterations in the mutated protein can be observed when comparing internal contacts (Fig. 6). In the wild type myocilin, the Thr394 residue interacts with Ala400 and Tyr376 by main-chain hydrogen bond and in the mutated protein, this residue keeps the hydrogen bond with Ala402 (in wild type myocilin, Ala400), but changes its interaction with Tyr376 to hydrophobic interaction. In addition, Thr394 also starts to interact hydrophobically with Lys400 and Gly401 by side-chain hydrogen bond. The residue Asp395 interacts by one main-chain hydrogen bond type with Lys400 and two main-chain hydrogen bonds with Ala399 in the normal myocilin. In the mutant myocilin, Asp395 preserves the interaction with Lys402 and loses it with Ala401. At the same time it interacts with Glu398 by main-chain hydrogen bond and with Pro397 (an inserted residue in the mutation) hydrophobically. In the wild type protein, the residue Glu396 interacts with Trp373 by main-chain hydrogen bond, with Glu323 by charge repulsive interaction, with Lys398 by main-chain hydrogen bond and two charge attractive interactions, and with Arg296 by two charge attractive interactions. However, in the mutant myocilin, Glu398 maintains only the main-chain hydrogen bond with Lys400 and establishes a new interaction with Gln368 by side-chain hydrogen bond and with Ala402, Gly401, Asp396 (an inserted residue in the mutation) and Asp395 by main-chain hydrogen bond. The residue Ala397 interacts with Gly399 by main-chain hydrogen bond and with Asp395 by side-chain and main-chain hydrogen bonds in the wild type myocilin. Nevertheless, in the mutant protein, only the interaction by hydrogen bond between Ala399 and Gly401 is maintained, and the new interaction is established by main-chain hydrogen bond between Ala399 and
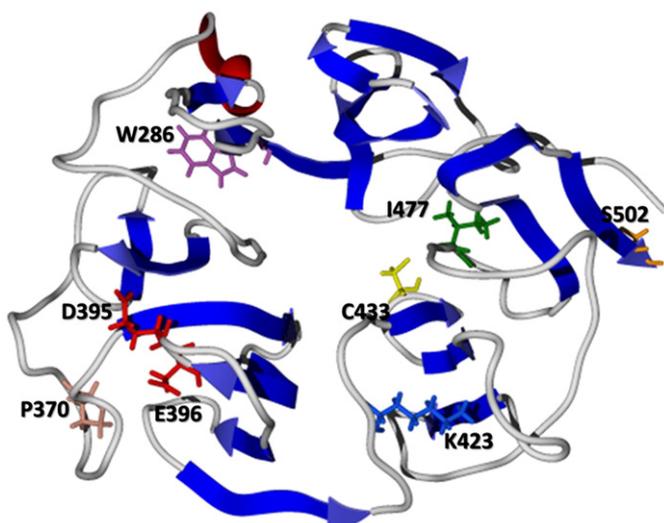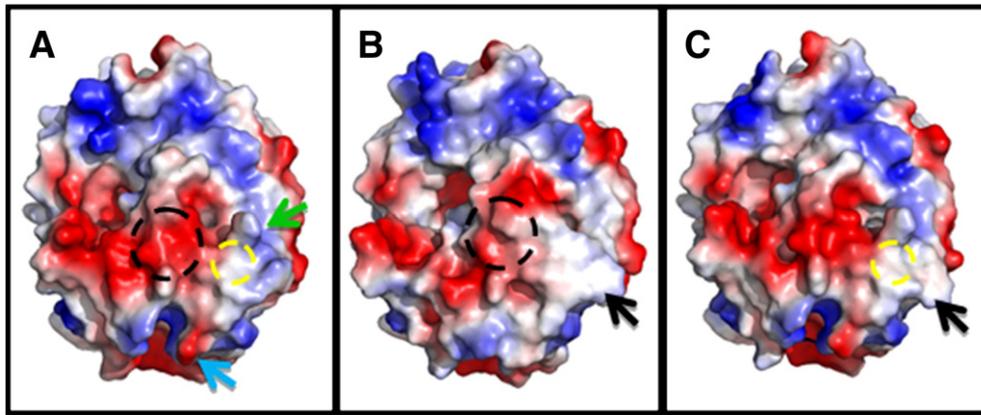
Fig. 5. Electrostatic potential surface map generated by PyMol for the modeled Olfactomedin domain of wild type myocilin (A) and the mutants p.D395_E396insDP (B) and p.P370L (C). The black circle indicates the position of p.D395_E396insDP insertion and the yellow circle indicates the position of p.P370L mutation. Black arrow indicates the neutral surface patch created upon mutations. Green and cyan arrows indicate position of Gln368 and Glu357, respectively.

Asp396 (an inserted residue in the mutation). Furthermore, the inserted residues increase the number of total interactions made by the mutated protein. The inserted residue Ala396 makes contact with Ala399, Glu398, and Trp373 by main-chain hydrogen bond and with Lys400 by two charge attractive interactions. Pro397, the other residue inserted in the mutation p.D395_E396insDP, makes contacts with Asp395 and Ser372 by hydrophobic interaction. Thus in total, the wild type myocilin makes 10 hydrogen bonds, two charge attractive and one charge repulsive interaction, while the mutant protein makes 15 hydrogen bonds, two charge attractive and five hydrophobic interactions.

4. Discussion

A novel mutation in the *MYOC* gene was reported that segregates with JOAG in a Brazilian family. It is an in-frame mutation, c.1187_ 1188insCCCAGA (p.D395_E396insDP), which leads to the insertion of six base pairs between the second and third bases of codon 396. Among disease-causing mutations categorized by type, small insertions comprise only 5.3% of the total variants reported (www.myocilin.com; Hewitt et al., 2008), and the c.1187_1188insCCCAGA insertion is probably involved in JOAG etiology in this family. This mutation does not change the myocilin sequence, except for the insertion of two residues,
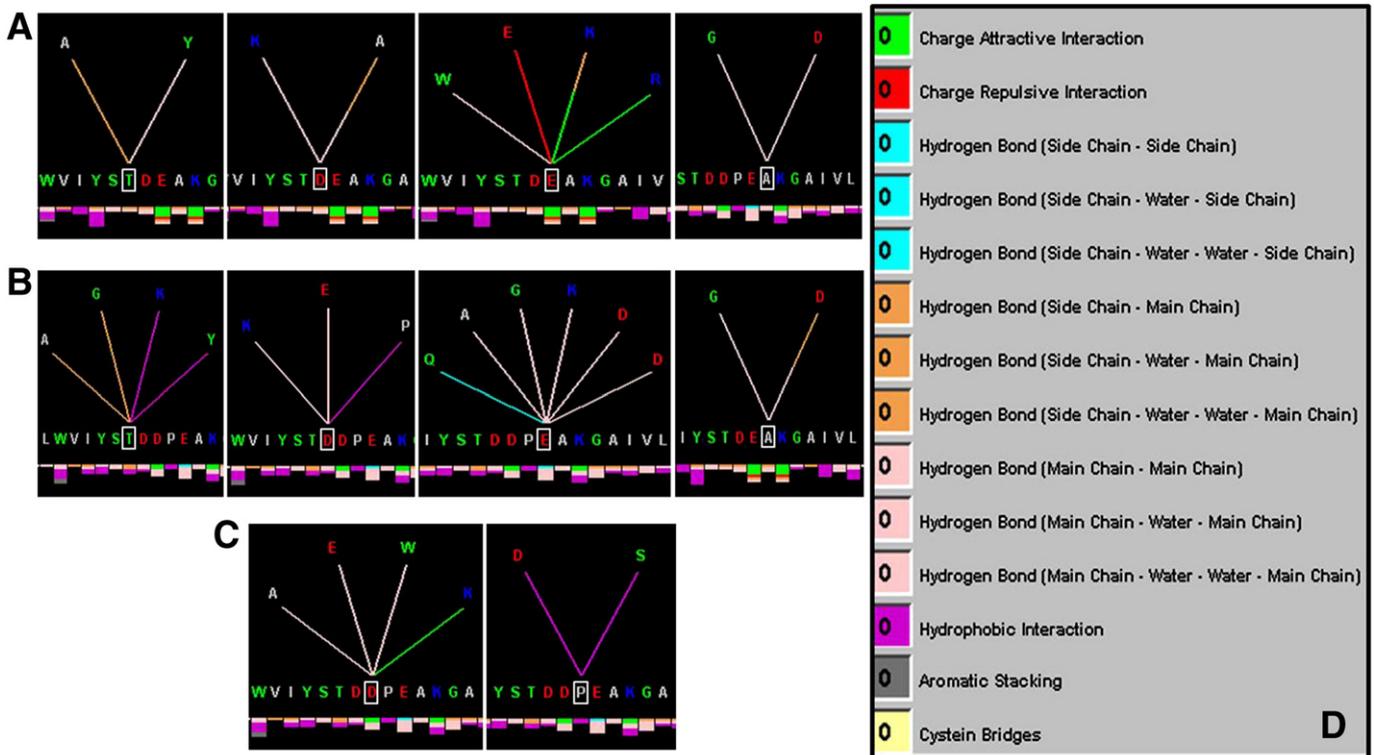

Fig. 6. Graphic of myocilin internal contacts generated by the STING Millennium Graphical Contacts program, showing the contacts made by the four residues (T, D, E and A) that flank the mutation in wild type (A) and mutant myocilin (B), as well as the contacts made by the residues inserted (C). In D, the color legend of the contacts.

aspartic acid and proline, between Asp395 and Glu396. A premature stop codon is not created by the insertion, suggesting the gain of function as a mechanism in glaucoma associated with the *MYOC* gene, which is the result of an abnormal property of mutant myocilin (Joe et al., 2003). Despite of the fact that residues Asp395 and Glu396 are not highly conserved among examined species, the mutation location is close to conserved regions among myocilin orthologs, and therefore, the insertion of the Asp and Pro residues might have caused significant changes in the mutated protein.

Structural modeling was performed using both threading and restraint-based molecular homology modeling. The modeling procedure was guided by threading suggestion and literature data. Recent circular dichroism results indicate that olfactomedin domain is composed mostly by antiparallel β-sheets and that there was no evidence for α-helices (Orwig and Lieberman, 2011). This is in disagreement with the myocilin model previously proposed in Kanagavalli et al.'s (2003) study. At the same time, this experimental evidence corroborates with the model proposed in the present work, indicating that it might be a better approximation to the real structure of myocilin olfactomedin-like domain. It is also possible that misfunction of myocilin protein is achieved by destabilization of internal contacts imposed by the mutation. Considering only the four residues that flank the insertion site, and inserted residues, there is a considerable difference between the internal contacts of the wild type and mutated protein. The increased number of hydrogen bonds and hydrophobic interactions may have caused changes not only in the mutation site, but in other locations of the mutated protein.

The p.D395_E396insDP results in the inclusion of Asp396 and Glu397 in the protein sequence. Structural analysis demonstrated that the in-frame insertion of two amino acids in the myocilin caused burial of charged and polar groups which may result in the exposition of a neutral patch on the surface of the olfactomedin domain. According to modeled structures, it is also possible that there was an increase in the surface hydrophobicity, favoring not only interactions with other proteins and myocilin itself but also aggregation. Another interesting feature observed was the reduced number of charge-repulsive contacts (from 13 in wild type to 5 in the insertion mutant), which may also account for misfunction and aggregation propensity (Münch and Bertolotti, 2010).

Gobeil et al. (2006) investigated the secretion status of the myocilin protein for 36 variants previously described in the *MYOC* gene. The authors observed that 20 mutations disturb myocilin secretion, and all of them encoded disease-causing proteins and carried mutations within the olfactomedin-like domain, including the p.396INS397 (www.myocilin.com; Hewitt et al., 2008) a duplication of three base pairs (c.1886_1888dup) that occurs very close to the mutation reported in the present study. According to those data, we can infer that the myocilin with p.D395_E396insDP mutation may have functional effect similar to those associated with the development of glaucoma, retained in the ER. Further functional studies would reveal if this mutation, such as many others in the *MYOC* gene (e.g., p.Q368X, p.P370L, p.K423E, p.C433R, and p.396INS397), leads to the intracellular sequestration (in the ER of trabecular meshwork cells) of insoluble aggregates of misfolded mutant myocilin, causing the death of these cells, and therefore impairing the aqueous humor outflow (Fautsch and Johnson, 2001; Jacobson et al., 2001).

About 8%–36% of JOAG cases and 3%–4% of adult-onset POAG cases are carriers of missense mutations in the *MYOC* gene (Fingert, 2011). Several investigations established good phenotype/genotype correlations for *MYOC* mutations. In the Brazilian population, the most common mutation is p.C433R, which is associated with severe glaucoma, including high penetrance before 40 years of age and IOP above 30 mmHg, as well as the frequent need for surgical intervention to control the disease progression. The age of onset in carriers of this mutation ranges from 17 to 58 years (Vasconcellos et al., 2003). The most common mutation in some populations, p.Q368X, has been associated with mean IOP of about 20–30 mmHg and the patients were diagnosed with OAG at an older adult age (www.myocilin.com; Hewitt et al., 2008). In the studied pedigree, we observed a milder phenotype of JOAG compared to other reported cases, as the carriers of p.P370L or p.Y437L mutations exhibited the early-onset form of the disease (in the first or second decades of life) and mean maximum IOP over 40 mmHg (Shimizu et al., 2000; Wiggs et al., 1998).

In our study, we observed complete penetrance after 30 years of age, with mean disease onset of 25 years (ranging from 20 to 30). Three of the four affected members had high IOP (28 to 47 mmHg) and a high cup-to-disc ratio (0.7 to 1.0), two are legally blind, and the other has a severe form of glaucoma with important visual field defects, which jeopardized the central vision at 23 years of age. The remaining member has a maximum IOP of 22 and 23 and cup-to-disc ratios of 0.2 and 0.3 in the RE and LE, respectively. There is an unaffected member of nine years old carrying the mutation and does not exhibit any symptoms of glaucoma. If he has no adequate clinical follow-up, this individual is at risk of developing glaucoma at a younger age. The lack of data about the structure of the myocilin protein increases the importance of functional studies as well as genotype–phenotype correlations, contributing to the knowledge of the role of the *MYOC* gene in glaucoma. In addition, in the translational medicine era, this study may help in the early diagnosis and proper assistance of other members within this family, as well as increasing the panel of *MYOC* mutations and their effects on phenotype.

References

Allingham, R.R., et al., 2005. Early adult-onset POAG linked to 15q11-13 using ordered subset analysis. Invest. Ophthalmol. Vis. Sci. 46, 2002–2005.

Baird, P.N., et al., 2005. Evidence for a novel glaucoma locus at chromosome 3p21–22. Hum. Genet. 117, 249–257.

Buchan, D.W., et al., 2010. Protein annotation and modelling servers at University College London. Nucleic Acids Res. 38, W563–568.

Carbone, M.A., et al., 2009. Overexpression of myocilin in the *Drosophila* eye activates the unfolded protein response: implications for glaucoma. PLoS One 4, e4216.

Chiti, F., et al., 2002. Studies of the aggregation of mutant proteins in vitro provide insights into the genetics of amyloid diseases. Proc. Natl. Acad. Sci. 4, 16419–16426.

Cuff, J.A., et al., 1998. Jpred: a consensus secondary structure prediction server. Bioinformatics 14, 892–893.

DeLano, 2002. The PyMOL Molecular Graphics System. DeLano Scientific, San Carlos, CA.

Fan, B.J., et al., 2006. Gene mapping for primary open angle glaucoma. Clin. Biochem. 39, 249–258.

Fautsch, M.P., Johnson, D.H., 2001. Characterization of myocilin–myocilin interactions. Invest. Ophthalmol. Vis. Sci. 42, 2324–2331.

Fingert, J.H., 2011. Primary open-angle glaucoma genes. Eye 25, 587–595.

Fingert, J.H., et al., 2011. Copy number variations on chromosome 12q14 in patients with normal tension glaucoma. Hum. Mol. Genet. 20, 2482–2494.

Gobeil, S., Letartre, L., Raymond, V., 2006. Functional analysis of the glaucoma-causing TIGR/myocilin protein: integrity of amino-terminal coiled-coil regions and olfactomedin homology domain is essential for extracellular adhesion and secretion. Exp. Eye Res. 82, 1017–1029.

Hewitt, A.W., Mackey, D.A., Craig, J.E., 2008. Myocilin allele-specific glaucoma phenotype database. Hum. Mutat. 29, 207–211.

Horwich, A., 2002. Protein aggregation in disease: a role for folding intermediates forming specific multimeric interactions. J. Clin. Invest. 110, 1221–1232.

Jacobson, N., et al., 2001. Non-secretion of mutant proteins of the glaucoma gene myocilin in cultured trabecular meshwork cells and in aqueous humor. Hum. Mol. Genet. 10, 117–125.

Joe, M.K., Tomarev, S.I., 2010. Expression of myocilin mutants sensitizes cells to oxidative stress-induced apoptosis: implication for glaucoma pathogenesis. Am. J. Pathol. 176, 2880–2890.

Joe, M.K., et al., 2003. Accumulation of mutant myocilins in ER leads to ER stress and potential cytotoxicity in human trabecular meshwork cells. Biochem. Biophys. Res. Commun. 312, 592–600.

Joe, M.K., Kee, C., Tomarev, S.I., 2012. Myocilin interacts with syntrophins and is member of dystrophin-associated protein complex. J. Biol. Chem. 287, 13216–13227.

Johnson, A.T., et al., 1993. Clinical features and linkage analysis of a family with autosomal dominant juvenile glaucoma. Ophthalmology 100, 524–529.

Kanagavalli, J., et al., 2003. Evaluation and understanding of myocilin mutations in Indian primary open angle glaucoma patients. Mol. Vis. 9, 606–614.

Kwon, H.S., Tomarev, S.I., 2011. Myocilin, a glaucoma-associated protein, promotes cell migration through activation of integrin-focal adhesion kinase–serine/threonine kinase signaling pathway. J. Cell. Physiol. 226, 3392–3402.

Kwon, H.S., et al., 2009. Myocilin is a modulator of Wnt signaling. Mol. Cell. Biol. 29, 2139–2154.

Lin, Y., et al., 2008. A genome-wide scan maps a novel autosomal dominant juvenile-onset open-angle glaucoma locus to 2p15–16. Mol. Vis. 14, 739–744.

Liu, Y., Vollrath, D., 2004. Reversal of mutant myocilin non-secretion and cell killing: implications for glaucoma. Hum. Mol. Genet. 13, 1193–1204.

Monemi, S., et al., 2005. Identification of a novel adult-onset primary open-angle glaucoma (POAG) gene on 5q22.1. Hum. Mol. Genet. 14, 725–733.

Münch, C., Bertolotti, A., 2010. Exposure of hydrophobic surfaces initiates aggregation of diverse ALS-causing superoxide dismutase-1 mutants. J. Mol. Biol. 399, 512–525.

Nagy, I., Trexler, M., Patthy, L., 2003. Expression and characterization of the olfactomedin domain of human myocilin. Biochem. Biophys. Res. Commun. 302, 554–561.

Neshich, G., et al., 2003. STING Millennium: a web-based suite of programs for comprehensive and simultaneous analysis of protein structure and sequence. Nucleic Acids Res. 31, 3386–3392.

Neshich, G., et al., 2004. JavaProtein Dossier: a novel web-based data visualization tool for comprehensive analysis of protein structure. Nucleic Acids Res. 32, W595–W601.

Neshich, G., et al., 2006. The Star STING server: a multiplatform environment for protein structure analysis. Genet. Mol. Res. 5, 717–722.

Neshich, G., et al. Surface Hydrophobicity Index (SHI): insights into the relationship between hydrophobic effect and oligomerization. Unpublished results.

Ortego, J., Escribano, J., Coca-Prados, M., 1997. Cloning and characterization of subtracted cDNAs from a human ciliary body library encoding TIGR, a protein involved in juvenile open angle glaucoma with homology to myosin and olfactomedin. FEBS Lett. 413, 349–353.

Orwig, S.D., Lieberman, R.L., 2011. Biophysical characterization of the olfactomedin domain of myocilin, an extracellular matrix protein implicated in inherited forms of glaucoma. PLoS One 6, e16347.

Pang, C.P., et al., 2006. A genome-wide scan maps a novel juvenile-onset primary open angle glaucoma locus to chromosome 5q. Mol. Vis. 12, 85–92.

Pasutto, F., et al., 2009. Heterozygous NTF4 mutations impairing neurotrophin-4 signaling in patients with primary open-angle glaucoma. Am. J. Hum. Genet. 85, 447–456.

Porter, L.F., et al., 2011. Identification of a novel locus for autosomal dominant primary open angle glaucoma on 4q35.1–q35.2. Invest. Ophthalmol. Vis. Sci. 52, 7859–7865.

Quigley, H.A., Broman, A.T., 2006. The number of people with glaucoma worldwide in 2010 and 2020. Br. J. Ophthalmol. 90, 262–267.

Quigley, H.A., Vitale, S., 1997. Models of open angle glaucoma prevalence and incidence in the United States. Invest. Ophthalmol. Vis. Sci. 38, 83–91.

Ray, K., Mukhopadhyay, A., Acharya, M., 2003. Recent advances in molecular genetics of glaucoma. Mol. Cell. Biochem. 253, 223–231.

Sali, A., Blundell, T.L., 1993. Comparative protein modelling by satisfaction of spatial restraints. J. Mol. Biol. 234, 779–815.

Sambrook, J., Fritsch, E.F., Maniatis, T., 1989. Molecular cloning: a laboratory manual, second ed. Cold Spring Harbor Press, Cold Spring Harbor (NY).

Sarfarazi, M., et al., 1998. Localization of the fourth locus (GLC1E) for adult-onset primary open-angle glaucoma to the 10p15–p14 region. Am. J. Hum. Genet. 62, 641–652.

Sheffield, V.C., et al., 1993. Genetic linkage of familial open angle glaucoma to chromosome 1q21–q31. Nat. Genet. 4, 47–50.

Shields, M.B., Ritch, R., Kruping, T., 1996. In: Ritch, R., Shields, M.B., Krupin, T. (Eds.), Classification of Glaucomas, second ed. vol. 2. Mosby-Year Book, Saint Louis, pp. 717–725.

Shimizu, S., et al., 2000. Age-dependent prevalence of mutations at the GLC1A locus in primary open-angle glaucoma. Am. J. Ophthalmol. 130, 165–177.

Sridharan, S., Nicholls, A., Honig, B., 1992. A new vertex algorithm to calculate solvent accessible surface area. Biophys. J. 61, A174.

Stoilova, D., 1996. Localization of a locus (GLC1B) for adult-onset primary open angle glaucoma to the 2cen-q13 region. Genomics 36, 142–150.

Stone, E.M., et al., 1997. Identification of a gene that causes primary open angle glaucoma. Science 275, 668–670.

Suntharalingam, A., et al., 2012. Glucose-regulated protein 94 triage of mutant myocilin through endoplasmic reticulum-associated degradation subverts a more efficient autophagic clearance mechanism. J. Biol. Chem. 287, 40661–40669.

Suriyapperuma, S.P., et al., 2007. A new locus (GLC1H) for adult-onset primary open-angle glaucoma maps to the 2p15–p16 region. Arch. Ophthalmol. 125, 86–92.

Thompson, J.D., Higgins, D.G., Gibson, T.J., 1994. CLUSTAL W: improving the sensitivity of progressive multiple sequence alignment through sequence weighting, position-specific gap penalties and weight matrix choice. Nucleic Acids Res. 22, 4673–4680.

Torrado, M., et al., 2002. Optimedin: a novel olfactomedin-related protein that interacts with myocilin. Hum. Mol. Genet. 11, 1291–1301.

Trifan, O.C., et al., 1998. A third locus (GLC1D) for adult-onset primary open-angle glaucoma maps to the 8q23 region. Am. J. Ophthalmol. 126, 17–28.

Ueda, J., Wentz-Hunter, K., Yue, B.Y., 2002. Distribution of myocilin and extracellular matrix components in the juxtacanalicular tissue of human eyes. Invest. Ophthalmol. Vis. Sci. 43, 1068–1076.

Vasconcellos, J.P.C., et al., 2003. Penetrance and phenotype of the Cys433Arg myocilin mutation in a family pedigree with primary open-angle glaucoma. J. Glaucoma 12, 104–107.

Wang, D.Y., et al., 2006. A genome-wide scan maps a novel juvenile-onset primary open-angle glaucoma locus to 15q. Invest. Ophthalmol. Vis. Sci. 47, 5315–5321.

Wiederstein, M., Sippl, M.J., 2007. ProSA-web: interactive web service for the recognition of errors in three-dimensional structures of proteins. Nucleic Acids Res. 35, W407–W410.

Wiggs, J.L., et al., 1995. Clinical features of five pedigrees genetically linked to the juvenile glaucoma locus on chromosome 1q21-a31. Ophthalmology 102, 1782–1789.

Wiggs, J.L., et al., 1996. The distinction between juvenile and adult-onset primary open-angle glaucoma. Am. J. Hum. Genet. 58, 243–244.

Wiggs, J.L., et al., 1998. Prevalence of mutations in TIGR/Myocilin in patients with adult and juvenile primary open-angle glaucoma. Am. J. Hum. Genet. 63, 1549–1552.

Wiggs, J.L., et al., 2004. A genomewide scan identifies novel early-onset primary open-angle glaucoma loci on 9q22 and 20p12. Am. J. Hum. Genet. 74, 1314–1320.

Wirtz, M.K., et al., 1997. Mapping a gene for adult-onset primary open-angle glaucoma to chromosome 3q. Am. J. Hum. Genet. 60, 296–304.

Wirtz, M.K., et al., 1999. GLC1F, a new primary open-angle glaucomalocus, maps to 7q35–q36. Arch. Ophthalmol. 117, 237–241.

Zhang, Y., 2007. Template-based modelling and free modelling by ITASSER in CASP7. Proteins 69, 108–117.

Zhou, Y., Grinchuk, O., Tomarev, S.I., 2008. Transgenic mice expressing the Tyr437His mutant of human myocilin protein develop glaucoma. Invest. Ophthalmol. Vis. Sci. 49, 1932–1939.

Zode, G.S., et al., 2012. Topical ocular sodium 4-phenylbutyrate rescues glaucoma in a myocilin mouse model of primary open-angle glaucoma. Invest. Ophthalmol. Vis. Sci. 53, 1557–1565.